PHYSICAL REVIEW B **73**, 180101(R) (2006)

Coarsening dynamics in elastically anisotropic alloys

B. Pfau,[1] L.-M. Stadler,[1] B. Sepiol,[1] R. Weinkamer,[2] J. W. Kantelhardt,[3] F. Zontone,[4] and G. Vogl[1]
[1]*Fakultät für Physik der Universität Wien, Strudlhofgasse 4, A-1090 Wien, Austria*
[2]*Max-Planck-Institute of Colloids and Interfaces, D-14424 Potsdam, Germany*
[3]*Fachbereich Physik, Martin-Luther-Universität, Halle-Wittenberg, D-06099 Halle (Saale), Germany*
[4]*European Synchrotron Radiation Facility—BP 220, F-38043 Grenoble Cedex, France*
(Received 19 December 2005; published 3 May 2006)

We study *in situ* the coarsening dynamics in elastically anisotropic phase-separating alloys, taking advantage of coherent x rays. Temporally fluctuating speckle intensities are analyzed for two different Ni-Al-Mo samples with different lattice misfits between precipitates and matrix. The detected long-term correlations depend not only on the norm but strongly on the direction of the scattering vector—an unambiguous proof of direction-dependent coarsening dynamics. For strong lattice misfits, our results indicate coalescence of precipitates in the {100} planes.

DOI: 10.1103/PhysRevB.73.180101 PACS number(s): 61.10.Eq, 05.40.−a, 81.05.Bx

Nickel-based superalloys are technologically important examples for elastically anisotropic phase-separating alloys, where precipitate coarsening is strongly influenced by long-range interactions due to lattice strains. The microstructural morphology, i.e., shape and alignment of the precipitates, and the coarsening kinetics have been heavily investigated in these systems, mainly using transmission electron microscopy (TEM) (Refs. 1–7), small-angle neutron scattering (SANS) (Refs. 5–7), and small angle x-ray scattering (SAXS) (Refs. 2 and 8). In the model system Ni-Al-Mo, $L1_2$-ordered Ni_3Al precipitates form, coherently embedded in an fcc nickel-rich matrix. The particle shape changes during growth from spherical to cuboidal and even to platelike for longer aging times. In addition, the precipitates are strongly aligned along the elastically soft ⟨100⟩ directions of the matrix. The magnitude of these effects is determined by the lattice misfit between the two phases, which is defined as $\delta=(a_p-a_m)/a_m$, with a_p and a_m the lattice parameter of the precipitates and the matrix, respectively. In Ni-Al-Mo alloys, δ can be controlled by the molybdenum content, which basically affects the lattice parameter of the matrix, a_m. It is thus possible to tune the misfit over a wide range, even from negative to positive values.

There is a number of theoretical attempts to study coarsening in elastically anisotropic alloys, see, e.g., Ref. 9 for a comprehensive review. The fundamental idea is the minimization of the sum of the interfacial energy and the elastic energy. With increasing size of a single particle the elastic energy increases faster and may become comparable or even larger than the interfacial energy, causing dramatic changes in the coarsening behavior. However, which mechanisms are responsible for coarsening under elastic strain remains undecided. Many studies[3,5,6,10] tried to verify coarsening via the classical Lifshitz-Slyozov-Wagner (LSW) mechanism, i.e., an evaporation-condensation mechanism, by following the coarsening kinetics, which is almost always done *ex situ*. For the LSW mechanism the particle growth is predicted to obey a power law for the mean particle radius, $\langle R\rangle$: $\langle R\rangle^\Lambda=\langle R_0\rangle^\Lambda+Kt$ with $\Lambda=3$ and K the coarsening rate. Alternatively to the LSW mechanism, the precipitates may migrate as a whole and coarsen by coalescence of particles, and a higher Λ exponent is predicted.[11]

Revealing the coarsening mechanism by fitting the above power law to the coarsening rate, derived from SAXS or TEM data, is difficult, since the sensitivity to the exact value of the exponent is not extremely high.[11] In Ref. 12 we presented a unique approach for discriminating between different coarsening mechanisms by applying the method of x-ray photon correlation spectroscopy (XPCS), taking advantage of coherent x rays that are available at third-generation synchrotrons. When scattered at disordered samples coherent radiation produces a highly modulated interference pattern. Since this so-called speckle pattern is in direct relation to the exact arrangement of the scattering centers in the coherently illuminated sample volume, the speckles will fluctuate if the scattering-center configuration changes. By analyzing the temporal correlations of the measured speckle-intensity fluctuations it is possible to gain information about the underlying dynamics in the sample. In order to study the very slow coarsening dynamics, the detrended fluctuation analysis (DFA) is applied. Originally developed for detecting long-range correlations in base-pair sequences in DNA (Ref. 13), the DFA method has proven to be ideally suited for analyzing persistent processes, with the climate as probably the most prominent example.[14] Furthermore, the DFA is capable to eliminate trends in the measurement data, caused, e.g., by small drifts in the experimental setup during long measurements, and to handle (slightly) nonstationary data.[15] A detailed discussion of DFA in the context of XPCS for determining coarsening dynamics in alloys is given in Ref. 16.

In the DFA the so-called fluctuation function, $F(t)$, is calculated as follows. First, the integrated time series, $Y(j)$, of the intensity fluctuations, ΔI_k, is calculated

$$Y(j)=\sum_{k=1}^{j}\Delta I_k,\ \text{where}\ \Delta I_k=I_k-\langle I\rangle \tag{1}$$

with I_k the intensity in the kth time step and $\langle I\rangle=(1/N)\Sigma_{k=1}^{N}I_k$ the mean intensity. Then $Y(j)$ is divided into nonoverlapping segments of size t, the scaling variable. In

each segment n with $Y[(n-1)t+1]$ to $Y(nt)$ a linear fit to the profile, $P_n(j)$, is performed and the variance

$$F_n^2(t) = \frac{1}{t} \sum_{j=(n-1)t+1}^{nt} [Y(j) - P_n(j)]^2 \quad (2)$$

is determined. Finally, $F_n^2(t)$ is averaged over all segments and the square root is taken to obtain the fluctuation function $F(t)$. To gain information about the correlations in the intensity fluctuations, the scaling behavior of the fluctuation function has to be analyzed. $F(t)$ is fitted by a power law, $F(t) \propto t^{\alpha}$, with α the fluctuation exponent, which is a measure for the degree of correlation or persistence in the system. In analogy to random walk theory, $\alpha = 1/2$ is found for uncorrelated data and $\alpha > 1/2$ for data containing long-term correlations.[15,17]

In simulations of coarsening in isotropic systems it turned out that the dependence of α on the norm of the scattering vector, $|\boldsymbol{Q}|$, is characteristic for different coarsening mechanisms,[18] as was verified experimentally in Ref. 12. Here we report on an XPCS investigation in dependence on both the norm and the *direction* of the scattering vector. XPCS is applied to follow *in situ* the coarsening dynamics in an elastically anisotropic phase-separating system. Results for Ni-Al-Mo are presented and compared with predictions from Monte Carlo (MC) simulations.

The XPCS measurements were performed at the high-brilliance undulator beamline ID10A at the ESRF, Grenoble, in SAXS transmission geometry with two alloys having different composition and, hence, different misfit. The composition (numbers indicate at. %) of the alloys were Ni-7.7Al-7.9Mo (alloy I) with almost negligible misfit ($\delta \approx -0.10\%$) and Ni-12.5Al-2.0Mo (alloy II) with $\delta \approx 0.65\%$ (Ref. 2). The misfit of alloy I is not high enough to form cuboidal precipitates.[2,3] After homogenizing and quenching into ice water the samples were annealed at 775 °C for 67.2 h (alloy I) and 164.5 h (alloy II), respectively. That treatment ensured a quasiequilibrium during the measurements, i.e., the mean SAXS signal did not change significantly.

An x-ray energy of 8 keV, corresponding to a wavelength of $\lambda = 1.55$ Å, was selected with a resolution of $\Delta E/E = 10^{-4}$, which provided the temporal coherence. To ensure spatial coherence a circular pinhole aperture of $d = 12$ μm diam was placed approximately 25 cm upstream the sample. Parasitic scattering from the pinhole was cut by guard slits between the sample and the pinhole. The *in situ* XPCS measurements of the $(\bar{1}10)$-oriented single-crystalline sample foils (thickness of 40–50 μm) were done with an evacuated furnace at 825 °C (alloy I) and 775 °C (alloy II), respectively.

In total, time series of $N = 6144$ pictures were taken with a repetition time of 2.7 s (1 s exposure, 1.7 s readout) using a direct illumination charged-coupled device (CCD) camera, $L = 1.9$ m downstream the sample. The expected speckle size ($\approx L\lambda/d = 23.8$ μm) corresponded to the CCD pixel size of 22.5 μm. The SAXS patterns of both samples averaged over 100 pictures with subtracted dark current are shown in Fig. 1. The pattern of alloy I [Fig. 1(a)] is characterized by an isotropic scattering intensity indicating isotropically distributed spherical precipitates with a mean radius of ≈50 nm. On the contrary, the SAXS signal of the second sample [Fig. 1(b)] exhibits a strong maximum in [001] which is due to both the precipitate shape and, much more important, due to the nearly periodic precipitate alignment in this direction. Assuming that the precipitates align in parallel sheets perpendicular to the ⟨100⟩ directions, as shown by Lund and Vooheers in three-dimensional reconstructions of scanning electron microscope pictures,[19] a mean sheet thickness of ≈100 nm and a mean sheet distance of ≈250 nm could be derived from the SAXS data.

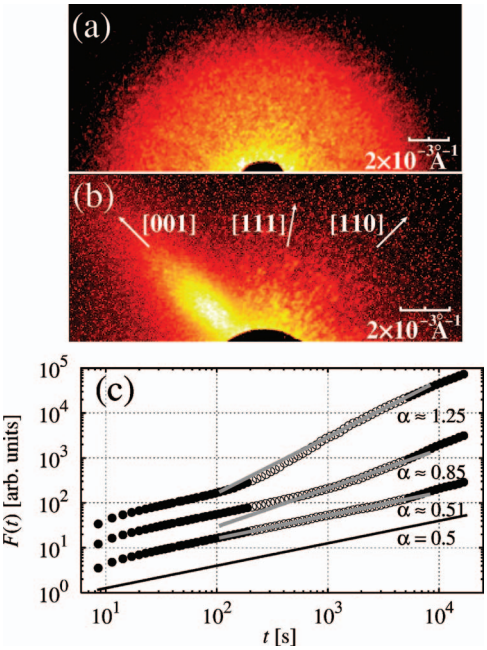

FIG. 1. (Color) Part of the SAXS patterns in the $(\bar{1}10)$ plane of (a) alloy I ($\delta \approx -0.1\%$) and (b) alloy II ($\delta \approx 0.65\%$) exhibiting pronounced speckles, logarithmic pseudocolor intensity scale. (c) Double-logarithmic plot of three typical fluctuation functions for alloy II at different $|\boldsymbol{Q}|$ along [001] ($|\mathbf{Q}|$ values from top to bottom: 6.7, 20.7, and 35.1×10^{-3} Å^{-1}). The sections of the fluctuation functions that were fitted by a power law $F(t) \propto t^{\alpha}$ (straight gray lines) are indicated by open circles. For the sake of clarity the fluctuation functions are shifted along the y axis and a $t^{1/2}$ line (corresponding to uncorrelated data) is shown for comparison.

The DFA was performed for different $|\boldsymbol{Q}|$ values along the main crystallographic directions [001], [110], and [111], whereby the fluctuation functions were averaged over 5 × 5 pixels to improve statistics. As shown in Fig. 1(c), the fluctuation functions were fitted by a power law $F(t) \propto t^{\alpha}$ on time scales with detectable correlations in the intensity fluctuations. The upper limit of the fit range was defined by 20% of the measurement time, where the DFA is still statistically reliable.[15] The lower limit was determined by the crossover from uncorrelated ($\alpha = 1/2$) to correlated behavior ($\alpha > 1/2$) in the fluctuation function for the smallest $|\boldsymbol{Q}|$ value and was held constant for all further $|\boldsymbol{Q}|$. The uncorrelated behavior on short time scales stems from the signal noise due to the limited intensity in the experiment.

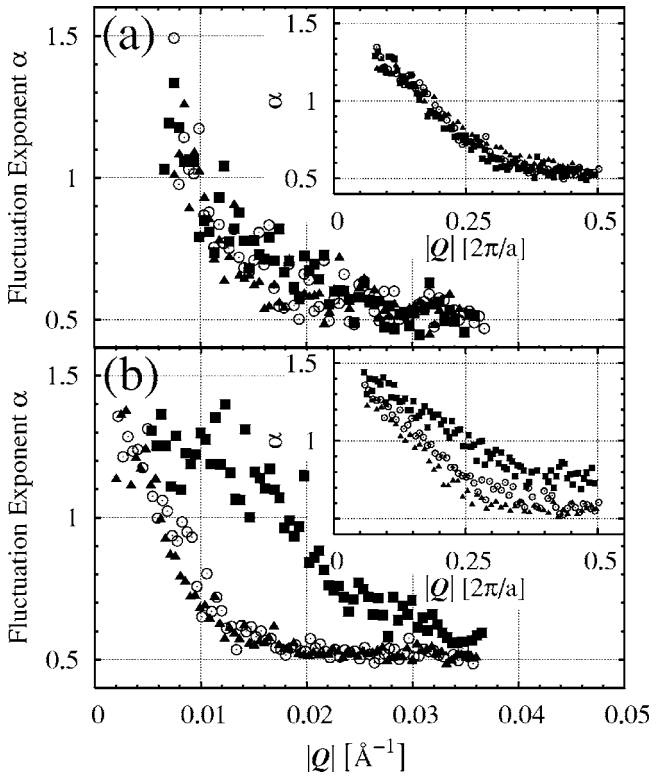

FIG. 2. Dependence of the fluctuation exponent α on the norm of the scattering vector, $|\boldsymbol{Q}|$, for (a) alloy I ($\delta=-0.1\%$) and (b) alloy II ($\delta=0.65\%$) along different crystallographic directions (■ [001], ⊙ [110], ▲ [111]). The α values were obtained by fitting the fluctuation functions with $F(t)\propto t^{\alpha}$. Error bars from fits are smaller than symbols. The insets show corresponding results from MC simulations, where precipitates are always much smaller compared to the experiment. In the simulation results the $|\boldsymbol{Q}|$ values are thus normalized relatively to the reciprocal lattice constant $(2\pi/a)$ in order to enable a qualitative comparison with the experimental results. Note the splitting of the $\alpha(|\boldsymbol{Q}|)$ curves in case of a strong misfit (b).

Figure 2 shows the collected fluctuation exponents α in the three crystallographic directions for both samples as a function of $|\boldsymbol{Q}|$. Differences in the coarsening behavior between the two samples and the different directions are very clearly observable. The $\alpha(|\boldsymbol{Q}|)$ curves can be understood within a simple picture: The higher the fluctuation exponent the more correlated the intensity fluctuations are in this $\boldsymbol{Q}$ range. The lower limit for α is $1/2$, implying only random uncorrelated fluctuations. Higher correlations in the signal result from rather monotonic increase or decrease of the measured intensity over longer time segments. Thus, $\alpha > 1/2$ can be interpreted as an enhanced structural persistence in the system. As a consequence, the particle configuration in the sample changes less on the specific length scale, corresponding to a certain value of $\boldsymbol{Q}$. Due to the quasiequilibrium condition it is obvious that on large length scales the configuration will be more persistent during the measurement, whereas very tiny structures will appear to evolve randomly due to elementary diffusion processes. Hence, the decrease of α with increasing scattering vectors is a common feature of all $\alpha(|\boldsymbol{Q}|)$ curves in Fig. 2.

In the case of alloy I with negligible misfit [Fig. 2(a)] no differences are visible in the $\alpha(|\boldsymbol{Q}|)$ curves for the different crystallographic directions, as expected, since the anisotropic elastic interactions do not take effect. But for alloy II [Fig. 2(b)] with high misfit the fluctuation exponents for the [001] direction exceed the exponents in the other directions significantly in the medium $|\boldsymbol{Q}|$ range. Thus, the dynamics in [001] is more persistent than in the other directions. This is an unambiguous proof of direction-dependent coarsening *dynamics* that has, to our best knowledge, never been reported in the literature.

Analogous to the evaluation of the experimental data speckle patterns computed in Monte Carlo (MC) simulations were analyzed. In the simulation model a coherent fcc lattice of the size of 96^3 unit cells with periodic boundary conditions is used. The lattice consists of two different types of atoms with different radii corresponding to the two phases of the alloy. Besides the classical "chemical" Ising interaction between nearest neighbors, an elastic energy is introduced depending on the displacement of an atom. A detailed model description and the exact numerical values can be found in Ref. 20. The simulations were performed with Kawasaki exchange dynamics for a model alloy with zero misfit, and an alloy with positive misfit ($\delta\approx 0.6\%$). The total simulation time was 2000 Monte Carlo steps (MCS), where one MCS is defined as one attempted exchange per atom. For the last 200 MCS the structure function of the lattice was calculated for every MCS. From these series of structure functions time series of simulated SAXS patterns were generated and analyzed using the DFA method.

The simulation results are shown as insets in Fig. 2. For coarsening of nonmisfitting particles a good qualitative agreement with the experiment is found, i.e., the $\alpha(|\boldsymbol{Q}|)$ curves show no dependence on the direction of the scattering vector. In the case of the high misfit alloy the characteristic splitting of the curves is well reproduced by the simulations, indicating dynamics with high persistence along [001]. Basically, a more quantitative agreement is hindered by the limited system size in the simulations that cause the precipitates to be much smaller than in the experiments.[21] In our simulations, the precipitates are furthermore not ordered and thus not separated by antiphase boundaries that also affect the coarsening behavior.[4,22,23] Finally, it is not straightforward to introduce vacancies in the used simulation model with Kawasaki dynamics, however vacancies are essential for the coarsening dynamics.[12,18]

Nevertheless the simulations are able to reproduce a microstructure [Fig. 3(a)], very similar to that observed in the TEM micrographs in Refs. 1, 2, and 7. In our investigations, the shape transition of the precipitates from cuboids to plates is of particular importance. The cuboidal precipitates are locally arranged on sheets in {100} planes[19] and grow to plates within these sheets. The plates form domains of a few parallel sheets[11] with hardly changing distances and thicknesses. This fixed structure explains the persistent configuration along the [001] direction, indicated by the high α values. As illustrated in Fig. 3(b) the precipitates have, on the other hand, a much higher mobility within the sheets and thus the $\alpha(|\boldsymbol{Q}|)$ curves decay very fast along the [110] direction. With the enhanced mobility the chance of precipitate coalescence as seen in simulations[24] and experiments[4–6] becomes reason-

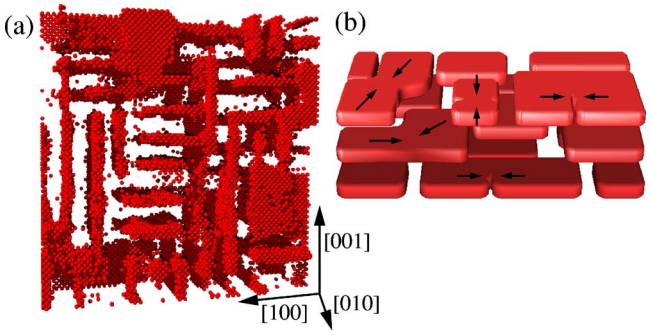

FIG. 3. (Color online) (a) Part of the simulation lattice ($50\times12\times50$ unit cells) after 2000 MCS. The precipitate atoms are drawn as spheres while the matrix atoms are not shown for the sake of clarity. The domains of parallel precipitate sheets in {100} planes are clearly visible. (b) Principle sketch for the precipitate dynamics. The precipitates lie and coarsen within stable planes. Within the planes the particles have a high mobility, which fosters coalescence. The shapes of the sample precipitates are inspired by simulations (Ref. 24) and TEM micrographs in Refs. 4–6.

ably high. Furthermore, the fast decay of the $\alpha(|\boldsymbol{Q}|)$ curves along [111] implies strong changes of the precipitate shape during coarsening, which is characteristic for precipitate coalescence.[12]

In conclusion, we successfully extended the method of x-ray photon correlation spectroscopy to a system with a completely anisotropic small-angle x-ray scattering pattern resulting from precipitates in an elastically anisotropic alloy. We thereby followed the coarsening dynamics *in situ*. In order to analyze the slow coarsening dynamics the technique of detrended fluctuation analysis was applied and the possibility of a fully $\boldsymbol{Q}$-dependent correlation analysis was demonstrated. The obtained strong dependence of the coarsening dynamics on the crystallographic direction—in particular the high persistence in [001]—is interpreted with almost exclusive coarsening within {100} planes. Our data provides strong evidence that coalescence plays an important role in forming platelike precipitates in elastically anisotropic alloys.

We thank O. Paris for providing the samples. This work was financially supported by the Austrian Federal Ministry for Education, Science and Culture (Project No. GZ45.529/2-VI/B/7a/2002), the Austrian Science Fund (FWF) (Project No. P17775-N02), and the EU Specific Targeted Research Project DYNASYNC (Project No. NMP4-CT-2003-001516). Data were evaluated using the Schrödinger II cluster of the Vienna University Computer Center.

[1] A. J. Ardell and R. B. Nicholson, Acta Metall. **14**, 1295 (1966).
[2] M. Fährmann, P. Fratzl, O. Paris, E. Fährmann, and W. C. Johnson, Acta Metall. Mater. **43**, 1007 (1995).
[3] J. G. Conley, M. E. Fine, and J. R. Weertman, Acta Metall. **37**, 1251 (1989).
[4] H. A. Calderon, J. G. Cabanas-Moreno, and T. Mori, Philos. Mag. Lett. **80**, 669 (2000).
[5] A. D. Sequeira, H. A. Calderon, and G. Kostorz, Scr. Metall. Mater. **30**, 7 (1994).
[6] A. D. Sequeira, H. A. Calderon, G. Kostorz, and J. S. Pedersen, Acta Metall. Mater. **43**, 3427 (1995); **43**, 3441 (1995).
[7] J.-M. Schneider, B. Schönfeld, B. Demé, and G. Kostorz, J. Appl. Crystallogr. **33**, 465 (2000).
[8] O. Paris, M. Fährmann, and P. Fratzl, Phys. Rev. Lett. **75**, 3458 (1995).
[9] P. Fratzl, O. Penrose, and L. Lebowitz, J. Stat. Phys. **95**, 1429 (1999).
[10] A. Baldan, J. Mater. Sci. **37**, 2171 (2002); **37**, 2379 (2002).
[11] R. Weinkamer, P. Fratzl, H. Gupta, O. Penrose, and J. L. Lebowitz, Phase Transitions **77**, 433 (2004).
[12] L.-M. Stadler, B. Sepiol, R. Weinkamer, M. Hartmann, P. Fratzl, J. W. Kantelhardt, F. Zontone, G. Grübel, and G. Vogl, Phys. Rev. B **68**, 180101(R) (2003).
[13] C.-K. Peng, S. V. Buldyrev, S. Havlin, M. Simons, H. E. Stanley, and A. L. Goldberger, Phys. Rev. E **49**, 1685 (1994).
[14] A. Bunde, J. F. Eichner, J. W. Kantelhardt, and S. Havlin, Phys. Rev. Lett. **94**, 048701 (2005).
[15] J. W. Kantelhardt, E. Koscielny-Bunde, H. H. A. Rego, S. Havlin, and A. Bunde, Physica A **295**, 441 (2001).
[16] L.-M. Stadler, B. Sepiol, B. Pfau, J. W. Kantelhardt, R. Weinkamer, and G. Vogl (unpublished).
[17] L.-M. Stadler, B. Sepiol, J. W. Kantelhardt, I. Zizak, G. Grübel, and G. Vogl, Phys. Rev. B **69**, 224301 (2004).
[18] R. Weinkamer and P. Fratzl, Europhys. Lett. **61**, 261 (2003).
[19] A. C. Lund and P. W. Voorhees, Acta Mater. **50**, 2585 (2002).
[20] H. Gupta, R. Weinkamer, P. Fratzl, and J. L. Lebowitz, Acta Mater. **49**, 53 (2001).
[21] Note that also the mean precipitate sizes of samples I and II differ significantly and since the $\alpha(|\boldsymbol{Q}|)$ curves for sample II cannot be scaled, a direct comparison with the ones for sample I is hindered.
[22] G. Rubin and A. G. Khachaturyan, Acta Mater. **47**, 1995 (1999).
[23] P. Nielaba, P. Fratzl, and J. L. Lebowitz, J. Stat. Phys. **95**, 23 (1999).
[24] J. Z. Zhu, T. Wang, A. J. Ardell, S. H. Zhou, Z. K. Liu, and L. Q. Chen, Acta Mater. **52**, 2837 (2004).